# Analysis of Compacted Semiflexible Polyanions Visualized by Atomic Force Microscopy: Influence of Chain Stiffness on the Morphologies of Polyelectrolyte Complexes†

**Gjertrud Maurstad, Signe Danielsen, and Bjørn T. Stokke***

*Biophysics and Medical Technology, Department of Physics, The Norwegian University of Science and Technology, NTNU, NO-7491 Trondheim, Norway*

*Received: October 11, 2002; In Final Form: December 30, 2002*

The morphologies of the compacted semiflexible biological polyanions alginate, acetan, circular plasmid DNA, and xanthan were investigated using tapping mode atomic force microscopy followed by quantitative image analysis. A shape factor was calculated for each of the observed polyelectrolyte complexes and used as a basis for dividing the structures into ensembles of morphologically linear, toroidal, and globular structures for subsequent quantitative analysis. Compaction of polyanions with chitosan yielded a small fraction of the torus morphology when the persistence length, $L_p$, of 25 nm (acetan) was reached. For both DNA, $L_p = 50$ nm, and xanthan, $L_p = 120$ nm, it was found that the toroids make up a substantial fraction of the complexed structures formed by the given chitosan and at room temperature. Rodlike complexes were additionally observed within DNA−chitosan complexes, whereas they do not appear as a significant fraction of chitosan-complexed high-molecular-weight xanthan. The average height of the condensates was observed to be ∼2 nm for the compacted xanthan toroids, while it was determined to be ∼5 nm for compacted DNA toroids. Reducing the degree of polymerization of xanthan yielded a decrease in the fraction of toroids. Compacted xanthan at room temperature displays a number of racquets and other morphologies similar to the reported intermediate, metastable states by simulations. The reduced abundance of such structures following annealing supports the interpretation of their metastable nature.

## Introduction

Linear polymers can undergo a transition from extended to a compact state driven by intersegment attraction and repulsion. In general, the detailed geometry of the compacted (bio)polymer structure varies from the sequentially organized polypeptide chains folding into structurally well-defined functional proteins, via clearly recognizable toroidal and linear compacted DNA, to compacted flexible polymers where the structure is not as clearly defined. The intersegment attraction in the self-assembly-driven compaction of polyelectrolytes, in particular studied for DNA, is mediated by multi- or polyvalent cations,[1−7] or cations used in combination with crowding or dehydrating compounds.[8,9]

The formation of the polyanion−polycation (polyelectrolyte) complexes is mainly driven by an electrostatic mechanism, where the exchange reaction of counterions with different valences is important.[10] Charge neutralization and possible local overcompensation or bridging mediated by a multivalent counterion induces attraction between topologically separated segments of the polyelectrolytes.[11] The valence of the counterion is a crucial factor for the efficiency of the complexation, concomitant compaction, and eventual stability of the compacted structure. The chain stiffness is identified as one important factor influencing the occurrence and abundance of the toroidal morphology of compacted semiflexible polymers[12,13] by opposing the formation of sharp bends.

The sequence-unspecific compaction of high-molecular-weight DNA observed using trivalent, e.g., cobalt hexamine,[2] or polyvalent, e.g., poly-L-lysine (PLL),[14] cations is reported to yield mainly toroidal and linear morphologies. The differences in stability of the toroidal state relative to the linear condensate and globular state is suggested to be due to the flexibility of the polymer at the same intersegment attraction energy. This has been investigated using theoretical methods as well as numerical simulations.[12,13,15−17]

In contrast to the relatively large parameter space of the intersegment attraction energy and chain stiffness explored in the theoretical and numerical work, there is less data available from the experimental side. There is a recent report of actin filaments forming toroidal condensates,[18] but apart from this most experimental work has focused on DNA compaction. DNA condensation has additionally been a strong motivation for many of the theoretical studies of polymer compaction. Here, we report on the compacted structures of different semiflexible polyanions chosen to span a range of persistence lengths, from 10 to 120 nm. The polyanions (alginate, acetan, plasmid DNA, and xanthan) are compacted using a polycation (chitosan or PLL). The structures are observed by tapping mode atomic force microscopy (AFM) and analyzed using the asymmetric properties of the individual species similar to that used in the numerical simulation of self-assembled polymers.[12,16] This approach is the basis for collecting complexes into different characteristic ensembles. Although selection of various polysaccharides allows control of the persistence lengths, the intersegment attraction energy associated with the complexation can vary concomitant with the chemical structure. The experimental conditions are selected in a range of polyanion−polycation concentrations, ionic strengths $I$, and pH values where complex formation is dominating the behavior. From simulations it is also suggested that compaction into toroidal condensates occurs through

† Part of the special issue "International Symposium on Polyelectrolytes".

* To whom correspondence should be addressed. Fax: +47 73 59 77 10. E-mail: bjorn.stokke@phys.ntnu.no.

10.1021/jp0271965 CCC: $25.00 
Published on Web 06/25/2003

**TABLE 1: Polyelectrolyte Samples Used for Polyelectrolyte Complex Formation**

| | $M_w$ | $b$ (nm) | p$K_a$ | $L_p$ (nm) |
|---|---|---|---|---|
| alginate[a,b] | $450 \times 10^3$ | 0.45[54,55] | 3.38 (ManA*p*)[56]<br>3.65 (GulA*p*)[56] | 5−17[31,32] |
| acetan | $2700 \times 10^3$ | 0.96[57] | | 30[30] |
| DNA | $2880 \times 10^3$ | 0.17[58] | 1[59] | 50[24−27] |
| xanthan | $5000 \times 10^3$, $400 \times 10^3$ [c] | 0.47[60] | 2.6−3.5[61,62] | 120[21] |
| chitosan[a] | | | 6.5[63] | 6−12[64] |
| $F_A = 0.1$ | $33 \times 10^3$ | 0.58[65] | | |
| $F_A = 0.49$ | $102 \times 10^3$ | 1.02 | | |
| $F_A = 0.15$ | $196 \times 10^3$ | 0.61 | | |
| poly-L-lysine | $540 \times 10^3$ | 0.38[66] | 10.68 | 1.8[66] |

[a] The fraction of ManA*p* (alginate) and Glc*p*NAc (chitosan) varies among different samples of these polysaccharides.[67−69] [b] For the alginate sample used, the fraction of α-GulA*p* ($F_G$) is 0.68. [c] A xanthan of reduced $M_w$ (by ultrasonication) was used in some of the experiments.

discrete intermediate states toward the thermodynamic stable state.[19,20] Some of our experimental observations will be discussed in view of these reported numerical simulations.

## Materials and Methods

**Biopolymer Samples.** The biological polyanions xanthan, DNA, acetan, and alginate were obtained and used for the polyanion−polycation complexation as follows. Xanthan, having a persistence length ($L_p$) equal to 120 nm,[21−23] is an extracellular polysaccharide produced by fermentation of *Xanthomonas campestris*. A 10 mL portion of a fermentation broth of xanthan (Statoil, Bioferm) was diluted to a total of 50 mL using 0.1 M NaCl, and centrifuged at 14000 rpm (Beckmann JA 21 rotor) for 60 min at 10 °C. The pellet was discarded and the polysaccharide precipitated from the supernatant by adding 2-propanol to equal amounts. The precipitate was redissolved in 0.1 M NaCl, and subsequently filtered using filters with pore sizes of 5.0 and 0.45 $\mu$m. Depolymerization to produce samples with different average chain lengths was carried out by treatment with ultrasound (Braun Labsonic 1510) at 50 or 100 W for 30 or 60 min. The samples were cooled on ice during the ultrasonication to avoid excessive heating. The plasmid DNA (pBR332, 4363 bp, Börhing Mannheim) was used without further purification. The parameter $L_p$ equals about 50 nm for linear DNA,[24−27] and will be used as an indicator of the chain stiffness of DNA although a circular plasmid is employed here.

Acetan (xylinan) is produced by a cellulose negative mutant of *Acetobacter xylinym*. The sample was purified,[28] and the dissolved freeze-dried material was determined to have a molecular weight $M_w = 2.8 \times 10^6$ using SEC-LALLS.[29] $L_p$ is reported to be 100 nm[28] at high $I$, and $L_p \cong 30$ nm in single-stranded conditions at low ionic strength.[30] Alginate from *Laminara hyperborea* stipe ($[\eta] = 14.4$ dL/g, $M_w \approx 450 \times 10^3$, FMC Biopolymers, Drammen, Norway) was used without further purification. The $L_p$ of alginate is reported to be between 5 and 17 nm.[31,32] Alginate stock solutions with polymer concentration $c_{alg} = 2.0$ mg/mL were prepared by hydration overnight. The chitosans were kindly provided by Dr. K. M. Vårum, Department of Biotechnology, NTNU, as freeze-dried material. Chitosans of different degrees of acetylation ($F_A$) as well as different degrees of polymerization (DP) were used. The chitosan was dissolved in 1% acetic acid at 1 mg/mL. A stock solution of poly-L-lysine ($M_w \approx 540 \times 10^3$, DP $\approx$ 2600, Sigma) was prepared by dissolution in milli-Q water. Table 1 summarizes the persistence lengths, molar masses, average distances between the charges in a line-charge model, $b$, and p$K_a$ values of the polyanion and polycation samples used in this study. Counterion condensation is expected for all the biopolymer samples with a $b$ parameter less than the Bjerrum length, $l_b = 0.71$ nm at room temperature.[33]

**Preparation of Polyelectrolyte Complexes.** Polyanion−polycation complexes were prepared in $NH_4Ac$ at different ionic strengths and pH 7.4 for DNA compaction; otherwise pH 5.5 was used. All polymers were further diluted in $NH_4Ac$ at the selected $I$ and pH before use, and the complexes were prepared by adding the polycation to the polyanion solution, at polyanion concentrations of 1−25 $\mu$g/mL. The samples were prepared for AFM imaging by transferring a 10 $\mu$L aliquot to a freshly cleaved 5 mm diameter mica disk, and after 1−2 min of incubation dried in a stream of $N_2$ followed by vacuum-drying at a pressure of $1.3 \times 10^{-4}$ Pa overnight. The DNA plasmid was dried using the same procedure, whereas the other uncomplexed polymers were prepared for imaging by AFM as described.[34,35] Preparation of complexes in aqueous NaCl yielded qualitatively the same structures as preparation in $NH_4Ac$. However, because NaCl forms salt crystals upon drying, and thereby obscures structures in the AFM topographs, the volatile salt $NH_4Ac$ was preferred for adjustment of the ionic strength.

**Atomic Force Microscopy.** AFM topographs of the polyelectrolyte complexes were obtained using a Digital Instruments Multimode IIIa atomic force microscope equipped with an E-scanner. Tapping mode silicon nitride cantilevers TESP (Digitial Instruments, Santa Barbara, CA) with nominal spring constants of 20−100 N/m and nominal resonance frequencies of 200−400 kHz were employed. The instrument was operated at a drive frequency less than the free oscillation resonance frequency, yielding 90% of the maximum amplitude. The topographs obtained at scan sizes in the range 1 $\mu$m × 1 $\mu$m to 5 $\mu$m × 5$\mu$m (512 × 512 pixels) were flattened line by line excluding the compacted structures prior to extraction of quantitative data.

**Image Analysis of AFM Topographs.** Dividing the polyelectrolyte complexes into linear, toroidal, and globular ensembles and determination of the contour length and height distributions of the polyelectrolyte complexes were carried out by image analysis of the AFM topographs. These analyses were carried out employing a user-interactive software developed in the IDL language (Research System, Inc., Boulder, CO). The algorithm described by Hoh and co-workers[36] was partly included to extract contour length data. Regions of interest (ROI), each containing one compacted structure, were obtained by thresholding and bileveling of the line-smoothed height topographs. The AFM height data were returned in the ROI, and a shape factor, the asphericity index $A$ (eq 1), was calculated

$$A = \frac{(\lambda_1^2 - \lambda_2^2)^2 + (\lambda_2^2 - \lambda_3^2)^2 + (\lambda_1^2 - \lambda_3^2)^2}{2(\lambda_1^2 + \lambda_2^2 + \lambda_3^2)^2} \quad (1)$$

for each of the species to guide the selection of species for the three ensembles.[37,38] The parameters $\lambda_i$, $i = 1-3$, are the eigenvalues of the tensor of the moment of inertia:

$$X_{\alpha,\beta} = \frac{1}{N}\sum_{i=1}^{N} S_i^{\alpha} S_i^{\beta}; \qquad \vec{S}_i = \vec{r}_i - \vec{R}_{CM}; \qquad \alpha, \beta = x, y, z \quad (2)$$

where $\vec{r}_i$ and $\vec{R}_{CM}$ are the positional coordinate of the pixel element $i$ in the structure and the center of mass of the structure, respectively. The height data were included in the calculations of $A$ by locating an element with a $z$ extension equal to the height at the half-height of the surface of the structure in each

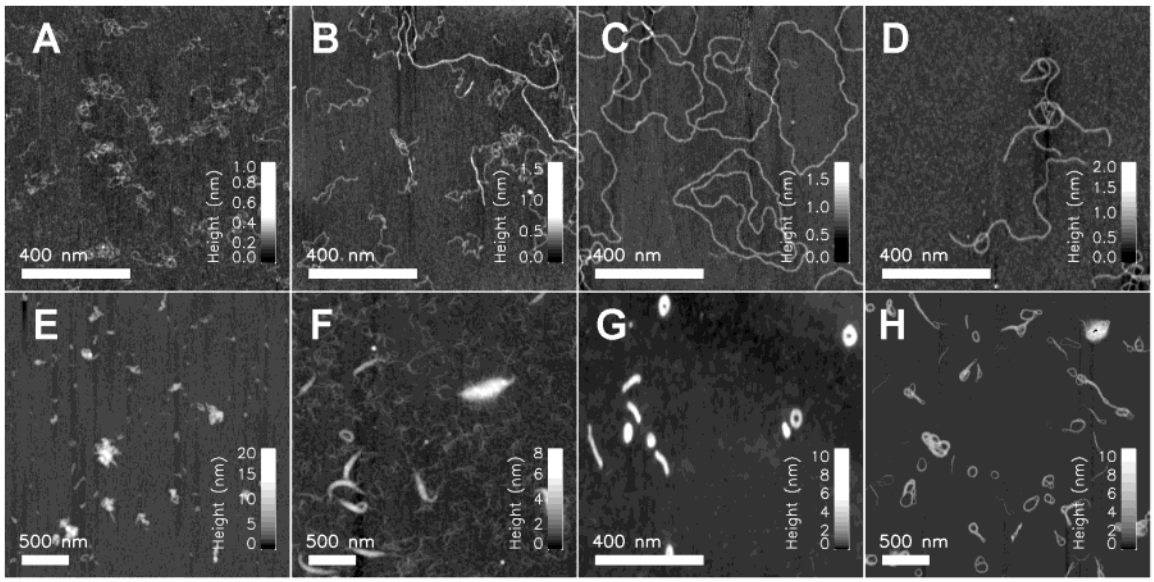


**Figure 1.** Tapping mode AFM height topographs of (A) alginate, (B) acetan, (C) DNA pBR332, (D) xanthan, and (E−H) the corresponding polyelectrolyte complexes with chitosan. A chitosan with a degree of acetylation of 0.1 and molecular weight of $33 \times 10^3$ was used to obtain the complexes shown in topographs E, F, and H, while a chitosan with a degree of acetylation equal to 0.15 and molecular weight of $196 \times 10^3$ was used for the complexes shown in topograph G. Experimental conditions were as follows: alginate−chitosan complexes at 150mM, pH 5.5, and $c_{alg} = 17\mu$g/mL; acetan−chitosan complexes at 20 mM, pH 5.5, and $c_{ace} = 25\ \mu$g/mL; DNA−chitosan complexes at 150 mM, pH 7.4, and $c_{DNA} = 4\ \mu$g/mL; xanthan−chitosan complexes at 5 mM, pH 5.5, and $c_{xan} = 2.5\mu$g/mL.

pixel and weighting the contribution to the tensor of the moment of inertia. The summation (eq 2) was therefore over each pixel element in the ROI.

The theoretical values of the asphericity index are $A = 0$, 0.25, and 1.0 for a sphere, an infinitely thin circle, and a rigid rod,[12] respectively, and were used as a basis for determination of ranges of $A$ to be used for assigning species to their respective ensembles. The contour lengths of the species in the linear ensemble were determined by thinning of the bileveled ROI, and returning pixel elements at the end of the thinned structure by back-extrapolation as described by Hoh and co-workers.[36] Branched species and species touching the edge of the topographs were excluded. The heights of the linear complexes were determined along the structures in the same thinned image used to determine the contour length. This method also allows determination of differences in heights within each complex.

Application of the thinning procedure to obtain the contour lengths of the toroidal structures often led to cutting of the circles even though smoothing was included before the bileveling. The contour lengths of the toroids were therefore obtained by determining the maximum height in the cross-section of the original image data returned to the ROI. These cross-sections were drawn radially from the center of the torus at incremental angles of 4° to cover the whole circumference. The circumference and height profiles of the species were obtained from these data. The number of species collected from several AFM topographs and included in each ensemble for the quantitative determination of the dimensions was in the range 50−100.

## Results and Discussion

**Observations of Polyelectrolyte Complexes.** The tapping mode atomic force microscopy (TM-AFM) topographs of the alginate, acetan, plasmid DNA, and xanthan ($M_w = 5 \times 10^6$), Figure 1A−D, respectively, show extended structures similar to those of earlier reported ultramicroscopic investigations.[30,39−41] The previously reported quantitatively determined chain stiffness from visualized chain trajectories of alginate and xanthan[30] is consistent with the persistence length of these polysaccharides in solution (Table 1). The employed preparation method is therefore found to preserve information about chain flexibility. Parts E−H of Figure 1 show examples of polyelectrolyte complexes of alginate, acetan, DNA, and xanthan, respectively, using chitosan as the polycation. These complexes were obtained at polyanion concentrations of 2.5−25 $\mu$g/mL. For alginate, acetan, and xanthan similar chitosan concentrations were used, while for DNA a chitosan concentration corresponding to a degree of neutralization of 0.9 of DNA was used. The concentration of the polycation was chosen such as to induce compaction of the polyanion. Different polycation concentrations were used because the charge density depends on the polyanions used. A lower polycation concentration corresponding to a polycation/polyanion charge ratio of 0.9 is required for DNA condensation. Varying the charge ratio between chitosan and DNA in the range 0.6−1.2 is found not to affect the geometries of the compacted structures.[42] Experiments at different polycation/polyanion charge ratios were also carried out with xanthan, acetan, and alginate. Most polyanions were observed to be condensed provided that the concentration ratio exceeded a lower threshold. A decreasing fraction of the polyanion was observed to be compacted below this threshold. Addition of excess polycations beyond the critical neutralization yielded a surplus of free chains observed separated from the complexes, while the geometry of the complexes was unaffected.

The AFM topographs of DNA−chitosan complexes reveal a blend of linear and toroidal structures similar to those reported for DNA−PLL complexes in distilled water and for DNA−spermidine complexes.[6,14,43] Complexation of a linear DNA with chitosan yielded compacted structures similar to those observed for the circular plasmid. Details of this and the influence of chitosan molecular parameters on the structure of the DNA−chitosan complexes will be presented elsewhere.[42] Complexation of DNA with chitosan at pH 5.5 reveals no major difference in geometry of the morphologies compared to that obtained at pH 7.4. The results obtained for DNA compaction at physiological pH are included here because of the relevance for application in gene therapy.

Increasing $L_p$ from 50 nm for DNA to 120 nm by changing the polyanion to xanthan reveals a blend of toroids, racquets with one or two loops at the end, and more complex self-assembled structures (Figure 1H). The main difference compared to the DNA−chitosan complexes is the nearly total absence of linear morphologies within the xanthan−chitosan complexes, and that it is mainly torus and racquet structures that can be observed. The complex species in this latter group are characterized by containing only a few sites with a small radius of curvature, i.e., no sharp turns. The structures of the xanthan−chitosan complexes were observed to be unaffected by an increase of $I$ from 5 to 20 mM. Increasing $I$ above 20 mM was found to yield an increasing extent of aggregation. This is in analogy with reports on DNA−PLL complexes, where complexes prepared in water were found to aggregate at increasing NaCl concentration.[14] Increasing the ionic strength using a monovalent salt is predicted to increase the charge reversal of the polyanion by a multivalent cation.[44] The overcharging is in general terms explained in terms of a correlation effect between the multivalent ions screening a macroion.[44] Appearing locally, this can be one molecular mechanism giving rise to aggregation of the complexes. Aggregation of polyelectrolyte complexes is also observed for a number of model systems, where small amounts of salt were found to have large effects on the aggregation behavior of complexes.[45] However, as aggregation is not observed for the DNA−chitosan complexes at $I = 150$ mM, there is a difference between the polyanions with respect to what ionic strength is required for formation of nonaggregating complexes. Additionally, initial observations of DNA−chitosan condensates obtained at lower ionic strengths indicate unchanged geometrical features of the toroids when the ionic strength is changed.

The appearance of uncomplexed acetan (Figure 1B) is similar to previous observations yielding $L_p = 30$ nm.[30] Increasing ionic strength was found to induce limited lateral chain association, apparently dimerization, that is considered consistent with $L_p = 100$ nm reported at higher ionic strengths.[28] The compacted structures obtained using polysaccharides with $L_p$ less than that of DNA yielded the following trends. Acetan−chitosan complexes of either toroidal or linear shapes were observed (Figure 1F). Their heights were somewhat larger than those observed for DNA−chitosan, with the linear complexes being higher than the circular complexes. The largest difference, however, was in the large fraction of uncomplexed acetan chains. Increasing the chitosan concentration did not qualitatively change this aspect. The relatively large fraction of uncomplexed acetan chains may be due to steric effects. The carboxylic group of acetan is located in the second residue relative to the backbone of the pentasaccharide side chain.[46] The regular grafting density of pentasaccharides on every second glucose backbone residue[46] indicates possible overlap between neighboring side chains, yielding steric hindrance toward polycations approaching the carboxylate. It is previously reported that $Cr^{3+}$-induced gelation of acetan is suppressed compared to that of xanthan, and that the $Cr^{3+}$-induced gelation is reestablished when the acetan pentasaccharide side chain is truncated toward the innermost disaccharide.[47] A similar steric effect affecting the acetan−chitosan electrostatic interaction is therefore possible. The acetan−chitosan complexes were not subjected to the quantitative analysis because of the relatively small fraction of chains being complexed.

The alginate−chitosan complexes (Figure 1E) prepared at $I = 150$ mM reveal apparent nontoroidal structures. A few of the structures were judged to be linear, but generally they appear with a less well-defined morphology than observed for the DNA−chitosan and xanthan−chitosan complexes. Toroids and racquets similar to those observed for compacted xanthan appeared as minor fractions at $I = 5$ and 20 mM. Most of the alginate chains appear to be included in the complexes. The finding of a small fraction of toroidal complexes at low ionic strength compared to essentially none at $I = 150$ mM may reflect the electrostatic contribution to $L_p$,[48] and the effect of chain stiffness on the morphologies of complex structures.[13] A similar sensitivity of ionic strength mediated by the electrostatic contribution to $L_p$ is not expected for the distribution of morphologies of the complexes of DNA and xanthan because of their larger structural $L_p$ (Table 1). Because most of the alginate−chitosan complexes were not of the same well-defined geometry as the linear and toroidal morphologies observed for DNA−chitosan and xanthan−chitosan, they were not included in the quantitative geometrical analysis.

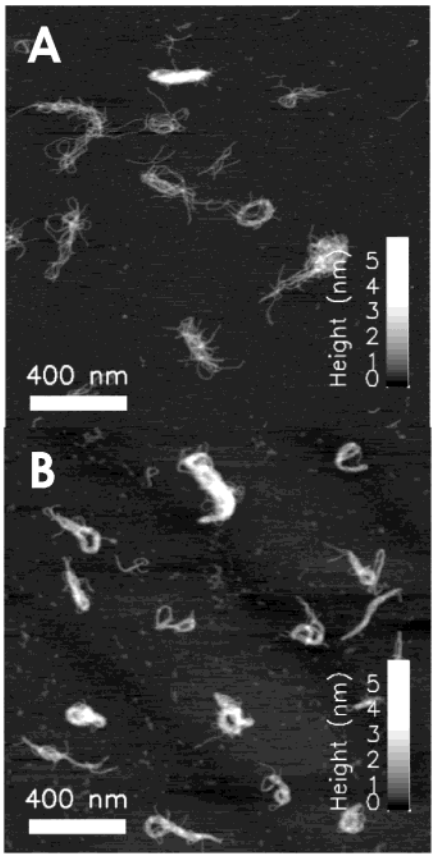


**Figure 2.** Tapping mode AFM height topographs of (A) acetan−PLL complexes and (B) xanthan−PLL complexes. In both cases a polyanion concentration of 1.5 $\mu$g/mL was used, and the complexes were prepared at 5 mM and pH 5.5.

Complexation of xanthan and acetan with PLL at $I = 5$ mM resulted in less well-defined geometrical structures and partly larger clusters (Figure 2) compared to those observed using chitosan. Reducing the total polyanion−polycation concentration during complexation did not yield any qualitative change in their size and appearance. Employing PLL as the polycation yielded more loosely compacted complexes than with chitosan, and several unbound polymer ends could clearly be identified emanating from each cluster. This feature indicates that there is more than one polyanion included in these complexes. Furthermore, the structures remained loose with free polymer ends when the PLL concentration was increased, in which case uncomplexed PLL could additionally be observed. The acetan−PLL complexes appeared similar to the xanthan−PLL structures

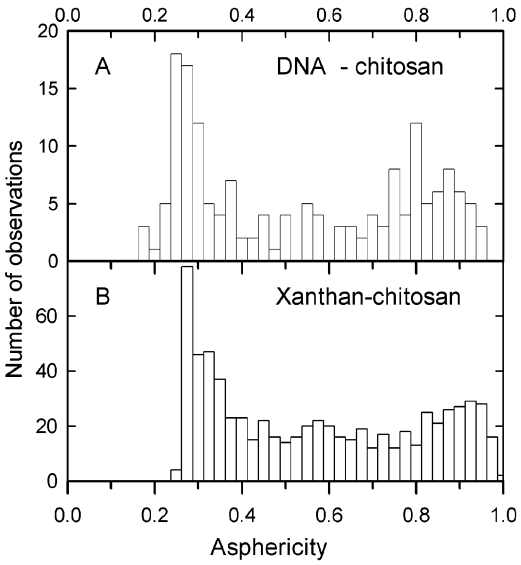


**Figure 3.** Distribution of the asphericity indices based on a number of AFM topographs for DNA−chitosan complexes ($M_{w,chit} = 196 \times 10^3$, 150 mM, pH 7.4, $c_{DNA} = 4$ $\mu$g/mL) and xanthan−chitosan complexes ($M_{w,chit} = 33 \times 10^3$, 20 mM, pH 5.5, $c_{xan} = 5$ $\mu$g/mL).

(Figure 2). This is in contrast to the observation of differences in the chitosan compaction of acetan and xanthan. The abundance of uncomplexed acetan chains observed with chitosan as the polycation was not observed for the acetan−PLL case (Figures 1 and 2). The pentasaccharide side chain of acetan appears not to represent steric hindrance for interaction with PLL as was the case for chitosan, yielding an apparent equilibrium that is shifted toward fewer uncomplexed acetan chains. The large flexibility of PLL as compared to chitosan (Table 1) is a possible molecular origin for this difference. The alginate−PLL complexes were observed to be more compact than the alginate−chitosan condensates using the same ionic strengths. At low $I$ (5 mM) the alginate−PLL complexes resembled the alginate−chitosan condensates at $I = 150$ mM.

No major difference in the morphologies of compacted xanthan and DNA 2 and 60 min after blending the solutions was observed. Complexes of xanthan−chitosan stored for 3 months were found to have both an unchanged fraction of toroids in the sample and the same dimensions of the toroidal complexes as the sample observed 30 min after initiation of the assembly process. These observations indicate no major change in the complex structures takes place after the initial 2 min. Furthermore, the sequence of mixing (polycation added to polyanion solution or vice versa) was found to affect neither the fraction of toroids nor their dimensions, in contrast to reports on DNA−PLL complexes.[14]

**Quantitative Analysis of the Polyelectrolyte Complex Morphologies.** Figure 3 shows the distributions of the asphericity indices $A$ for DNA−chitosan and xanthan−chitosan complexes. More than 100 complexes collected from several AFM topographs were included in the distributions. These distributions reveal a peak centered around $A = 0.25-0.30$ and a broad shoulder extending up to $A = 1.0$. The shoulder in the case of DNA−chitosan has a second maximum for the actual conditions for preparation of the complexes, centered around $A = 0.8-0.9$. The peak at $A = 0.25-0.30$ is expected from the theoretical analysis[12] to contain only the toroids. Identification of the species within this peak reveals that this is the case for the xanthan−chitosan complexes, whereas this peak additionally includes the globular species of DNA−chitosan. The reason that

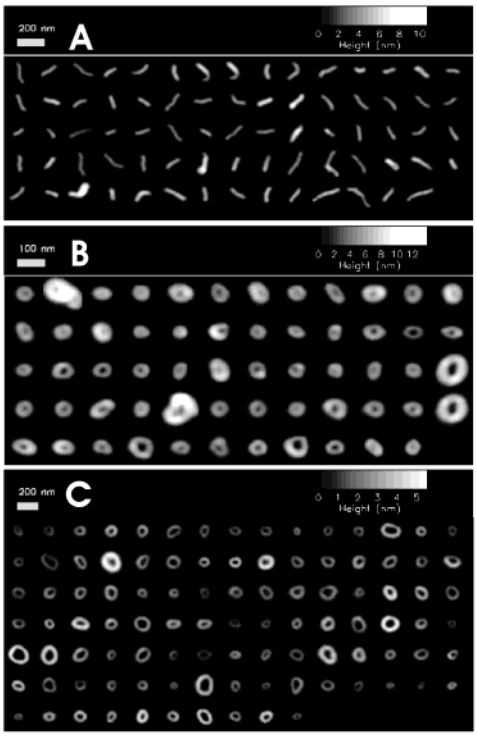


**Figure 4.** Image galleries of ensembles of (A) toroidal and (B) linear DNA−chitosan complexes ($M_{w,chit} = 196 \times 10^3$, 150 mM, pH 7.4, $c_{DNA} = 4$ $\mu$g/mL) and (C) toroidal xanthan−chitosan complexes ($M_{w,chit} = 33 \times 10^3$, 20 mM, pH 5.5, $c_{xan} = 5$ $\mu$g/mL). Species were selected for the toroidal ensembles for asphericity index in the interval $0.2 < A < 0.35$ and the linear ensemble when $A > 0.5$.

the globular species do not yield the expected $A = 0$ is most likely due to the convolution of the atomic force microscope tip with the structure. The image of a spherical structure with radius less than the radius of curvature of the atomic force microscope tip will appear with a diameter much larger than the true diameter. Furthermore, it was found that the distribution of $A$ in the range 0.6−1.0 contained both the expected morphologically linear, curved complexes and the racquets observed for xanthan−chitosan complexes. Thus, the asphericity index did not resolve the racquet structures as uniquely identifiable species. Despite these overlapping regions, the distributions of the asphericity indices provide some insight into the relative abundance of the various morphologies observed within a sample of polyelectrolyte complexes, and were used to guide the manual selection of the complexes for three morphologically distinct ensembles for further analysis. Complexes were included in the toroidal ensemble provided that $A \in 0.2-0.35$, i.e., close to the ideal torus, and that there was a distinct hole in the center following the thresholding procedure. The globular ensemble was selected to consist of complexes with $A \in 0.0-0.50$ and with no clear height minimum centrally located in the species. The linear ensemble consisted of complexes with $A \in 0.5-1.0$ excluding racquet structures.

Figure 4 shows image galleries of the species in circular and linear ensembles of DNA−chitosan complexes (Figure 4A,B) and a circular ensemble of xanthan−chitosan complexes (Figure 4C). The linear and circular ensembles for DNA−chitosan constitute about 90% of the total number of species observed in the AFM topographs for this particular case. The globular species do not represent a large fraction for the selected chitosan, and the remaining complexes do not fit into any of the three selected categories. The circular ensemble constitutes about 20% of the xanthan−chitosan complexes. The circular ensemble is

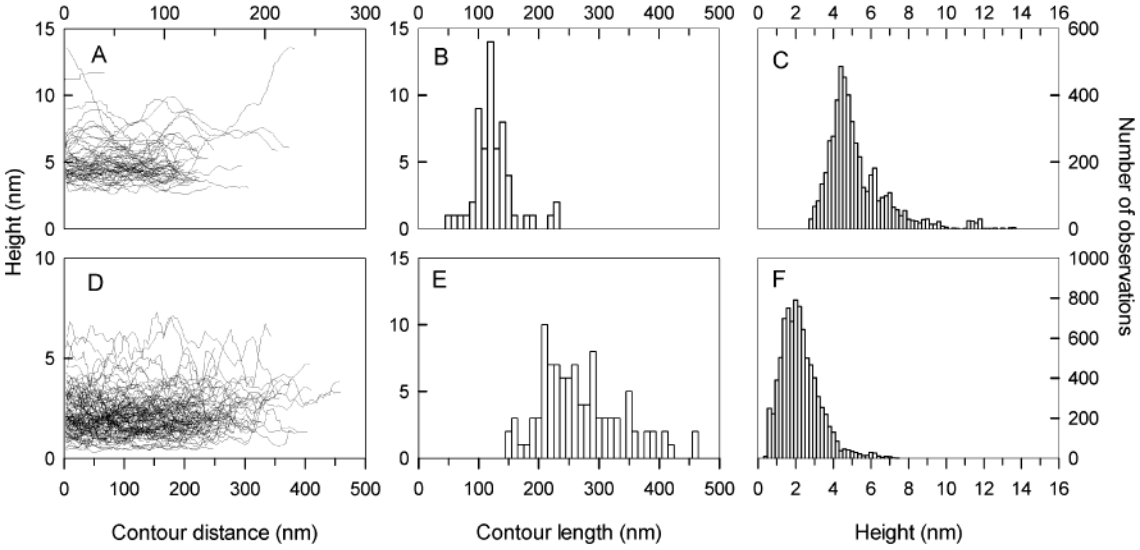


**Figure 5.** Height vs contour distance and distributions of the contour length and the height for the toroidal complexes of DNA−chitosan ($M_{w,chit} = 196 \times 10^3$, 150 mM, pH 7.4, $c_{DNA} = 4$ $\mu$g/mL) (A−C) and xanthan−chitosan ($M_{w,chit} = 33 \times 10^3$, 20 mM, pH 5.5, $c_{xan} = 5$ $\mu$g/mL) (D−F).

**TABLE 2: Dimensions and Fraction of Toroids of DNA−Chitosan and Xanthan−Chitosan Polyelectrolyte Complexes**

| polyanion | chitosan | $I$ (mM) | $\langle h \rangle_{tor}$ (nm) | $\langle L_C \rangle_{tor}$ (nm) | fraction of toroids (%) |
|---|---|---|---|---|---|
| DNA | $F_A = 0.15$, $M_w = 196 \times 10^3$ | 150 | 5.1 | 120 | 40 |
| xanthan $M_w = 5 \times 10^6$ | $F_A = 0.1$, $M_w = 33 \times 10^3$ | 5 | 2.2 | 260 | 21 |
| $M_w = 5 \times 10^6$ | $F_A = 0.1$, $M_w = 33 \times 10^3$ | 20 | 2.2 | 263 | 30 |
| $M_w = 5 \times 10^6$ | $F_A = 0.49$, $M_w = 102 \times 10^3$ | 5 | 2.1 | 298 | 28 |
| $M_w = 5 \times 10^6$ | $F_A = 0.49$, $M_w = 102 \times 10^3$ | 20 | 1.6 | 277 | 24 |
| $M_w = 0.4 \times 10^6$ | $F_A = 0.1$, $M_w = 33 \times 10^3$ | 5 | 2.0 | 253 | 6 |
| $M_w = 5 \times 10^6$ | $F_A = 0.49$, $M_w = 102 \times 10^3$ | 20 | 3.5[a] | 295[a] | 52[a] |

[a] The sample was heat treated at 50 °C for 3 h after the complexation at room temperature.

of particular interest because the quantitative data will be used for discussion of intersegment attraction energy in the following.

Figure 5 shows the height along the contours within the species and distributions of the heights and contour lengths for the circular ensemble of DNA−chitosan (Figure 5A−C) and xanthan−chitosan toroidal complexes (Figure 5D−F). The individual height profiles indicate possible coexistence of different heights within a single complex. The length distributions of the circular DNA complexes show an average length of 120 ± 35 nm. A similar contour length is observed for the rodlike morphologies of the complexes (125 ± 37 nm, distribution data not shown). These values are about 8% of the contour length of the uncomplexed plasmid (Figure 1). The height distributions collected from tracing the contours reveal a main peak with a most abundant height of 4.5 nm for the toroidal complexes. Additionally, there is a tail extending up to 15 nm. For xanthan−chitosan complexes, only defect-free toroids are included in the circular ensemble. In addition to these a smaller fraction of imperfect toroids were observed. These imperfections typically appeared as being formed from a bent racquet with an open head, or loop, and structures resembling pretzels, in which the formation of a toroid appeared not to have reached completion. The xanthan−chitosan toroids are 263 ± 68 nm long, with an average height of 2.2 nm, the tail of the height distribution extending up to 8 nm. The mean dimensions of the observed toroids and the fraction of these species were unchanged when a chitosan with $F_A = 0.1$ or $F_A = 0.49$ was used for compaction of xanthan (Table 2).

**The Xanthan Chain Length Affects the Morphologies of Xanthan−Chitosan Complexes.** Parts A and B of Figure 6 illustrate the effect of the degree of polymerization of xanthan on the morphology of the polyelectrolyte complexes. The racquet morphologies with loops at one or both ends become less abundant and eventually cease to exist as the chain length is reduced. The loss of the racquet structures is not clearly apparent in the asphericity distribution, because of the overlap with rods in the $A \in 0.5-1.0$ region. Additionally, the fraction of toroids is reduced, yielding a species distribution almost depleted (3−8%) in these structures for the depolymerized sample. The distribution of the morphologies is dominated by rods, and few, if any, toroids are present at a sufficiently low degree of polymerization. A reduction in $M_w$ from $5 \times 10^6$ to $0.4 \times 10^6$, where the toroidal fraction is reduced significantly (Figure 7), illustrates this point. These observations are analogous to experimental results on DNA condensation where the lower boundary of 400 bp needed for toroidal formation is reported.[1] Additionally, the data on compaction of xanthan indicate the geometries of the compacted toroids for the two molar masses of xanthan also are independent of the two ionic strengths, and not influenced by the selection of the chitosan

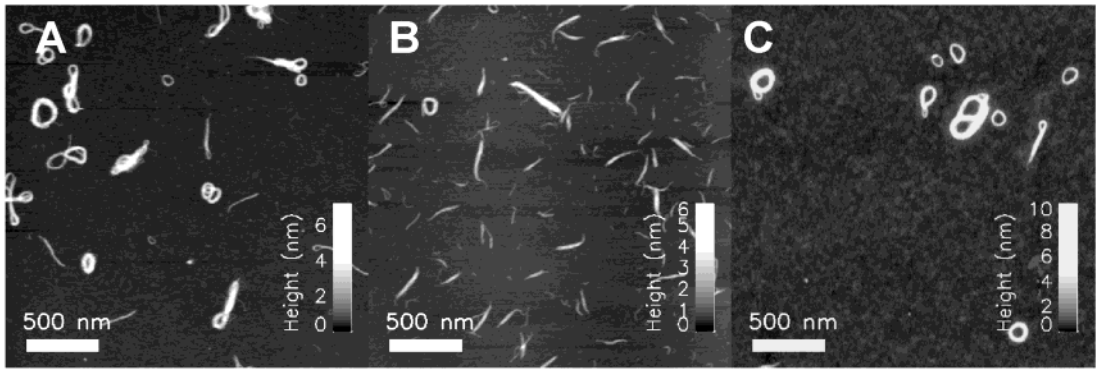


**Figure 6.** Effect of the degree of polymerization of xanthan on the complex morphology, illustrated by AFM height topographs: (A) complexes prepared from $M_w = 5 \times 10^6$ xanthan and (B) $M_w = 0.4 \times 10^6$ xanthan; (C) complexes prepared from $M_w = 5 \times 10^6$ xanthan at room temperature and annealed at 50 °C for 3 h. For the experiments on the effect of DP a chitosan of molecular weight $33 \times 10^3$ was applied, and complexes were prepared at an $I$ of 5 mM and pH 5.5. The concentration of xanthan is 2.5 $\mu$g/mL (A) and 1.5 $\mu$g/mL (B). For the effect of annealing a chitosan of molecular weight $102 \times 10^3$, $I = 20$ mM, pH 5.5, and xanthan concentration 2 $\mu$g/mL (C) were used.

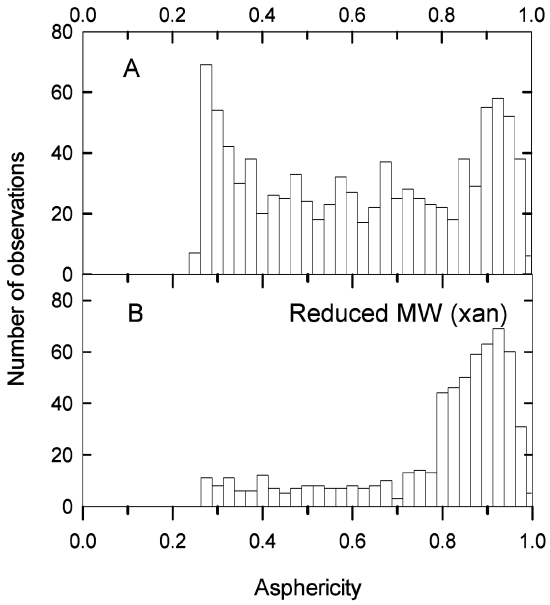


**Figure 7.** Comparison of asphericity distributions for xanthan−chitosan complexes prepared from xanthan with $M_w = 5 \times 10^6$ (A) and $0.4 \times 10^6$ (B). Examples of AFM topographs are shown in Figure 6A,B, and the conditions used are detailed there.

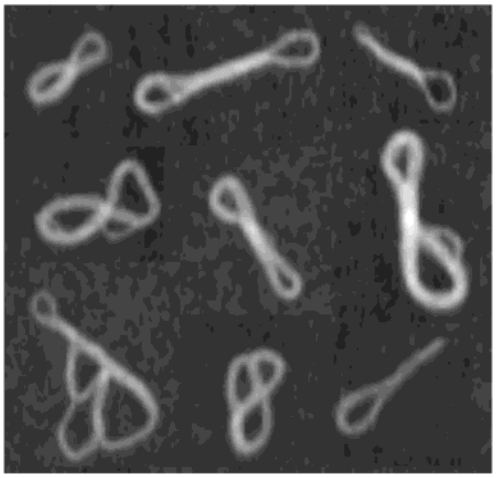

**Figure 8.** Examples of the metastable structures observed among xanthan−chitosan complexes ($M_{w,chit} = 33 \times 10^3$, 20 mM, pH 5.5, $c_{xan} = 5$ $\mu$g/mL).

(Table 2). The few toroids formed consist most likely of chains from the upper tail in the chain length distribution of this depolymerized xanthan sample.

**Intermediate, Metastable States of Xanthan−Chitosan Polyelectrolyte Complexes.** Figure 8 shows selected examples of racquet-shaped structures (rods with one or two loops at the ends) typically observed for xanthan−chitosan complexes. In addition to these, a number of other morphologies with additional interconnected loops are also observed for compacted xanthan. These experimentally observed structures resemble to a great extent those reported using Brownian dynamics simulation of the kinetic pathway of polymer collapse.[20,49] It was reported that the evolution progresses through a number of states, typically four different conformations: the extended chain, single-headed racquets, multiple-headed racquets, and torus. The experimentally observed structures (Figure 8) are similar in appearance to the intermediate, metastable states trapped by large energy barriers on the pathway toward the toroidal, thermodynamically stable state. Metastable structures with loops clearly seen at the ends of the structures are expected for rather stiff polymers, as the bending energy associated with forming a smaller loop would be larger. These structures make up a substantial fraction of the complexes for xanthan−chitosan condensates formed at room temperature.

Annealing of the aqueous xanthan−chitosan complexes was carried out to reduce the fraction of species in the apparently metastable state and drive the system closer to equilibrium. Heating of the complexes (50 °C, ∼3 h) led to an increase in the fraction of toroids from 24% to 52% and a concomitant reduction in the number of racquets. Moreover, the average circumference of the complexes was unaffected by the heat treatment, whereas the mean height of the structures increased from 1.6 to 3.5 nm (Figure 7C and Table 2). The height distribution indicates that the annealing yielded a selective increase in the height distribution in the height range 3−6 nm while the range 1−2 nm was less affected (Figure 9). In view of the reduction of the fraction of the metastable structures, it is suggested that the metastable states mainly consist of the high-molecular-weight tail of the xanthan chain distribution. These are transformed to toroidal structures with a larger number of windings than those formed at room temperature. This interpretation is also supported by the high-molecular-weight tails allowing a larger number of intersegment interactions in the metastable state than shorter chains would, so these high-molecular-weight species are more easily trapped in intermediate states. The particular experimental condition used in this example was selected to keep the xanthan in the ordered conformation during the annealing. Preliminary investigations of

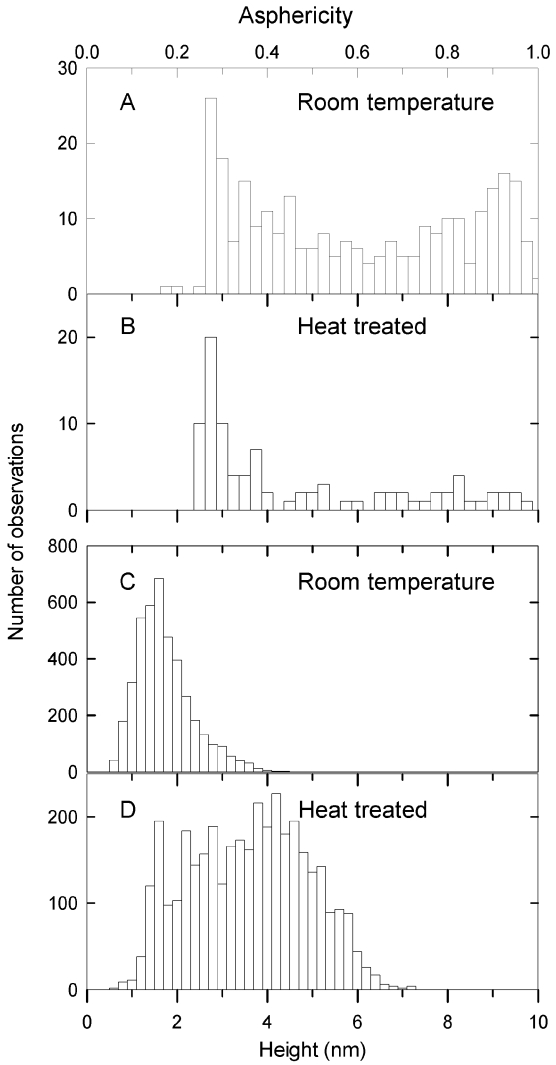


**Figure 9.** Asphericity distributions (A, B) and height distributions of the toroids (C, D) of xanthan−chitosan polyelectrolyte complexes before (A, C) and after (B, D) annealing. An example of an AFM topograph after annealing of the xanthan−chitosan complexes is shown in Figure 6C.

annealing effects of xanthan−chitosan complexes at conditions inducing the disordered conformation and return to the ordered conformation after cooling yield a more complicated picture. The interplay between the conformational transition of xanthan and changes during annealing of polycation-compacted xanthan is subject to further investigations and will be reported later.

**Possible Influence of Chain Stiffness on the Morphologies of Polyelectrolyte Complexes.** Theoretical methods have established a phase diagram of the collapse transition of semiflexible polymers.[13] The $L_p$ parameter is in this context found to be important in determining the collapsed structure. Similarily, theoretical calculations on the morphologies of condensed DNA also include chain stiffness as one important factor.[50] The use of the semiflexible biopolymers xanthan, DNA, and alginate here, which all form complexes with chitosan, yields a certain basis for comparison to the theoretical work. The present data do not support determination of a transition between the various states, in particular because it is difficult to tune the intersegment attraction continuously. Despite this limitation, some indication of three existing states emerges: the coil, the torus, and the globule. On the basis of the qualitative appearance, the alginate−chitosan complexes are found within the globular region, while chitosan complexes of DNA and xanthan are in the toroidal region. The transitions between the regions are not sharply defined, but might be regions of coexistence of various structures, where, for example, the rods occur.[13] Compacted DNA yields a significant fraction of rods and apparently globular condensates in addition to the toroids.

The ratios between the mean circumference of the compacted toroids and the persistence length of both compacted xanthan and DNA using chitosan are both about 2.4. This is only slightly less than the optimum of the cyclization probability of semiflexible polymers,[51] and may indicate that these toroids are folded to these dimensions as a consequence of the dynamic flexibility of the chains. Studies of linear DNA inserted with a particular base sequence indicate that local static curvature may dominate the toroids being formed at an early stage of the condensation.[52] Later in the complexation reaction, toroids of the size induced by the dynamic curvature dominate the population. This additional information may indicate that the chitosan−DNA and chitosan−xanthan interactions do not affect local curvature to a large extent and allow toroid formation dominated by the fluctuations allowed by the chain stiffness of the polyanion.

## Conclusion

In this paper, the morphologies of compacted structures of semiflexible biopolymers obtained by polyanion−polycation complexation were studied by direct visualization of the structures using tapping mode atomic force microscopy of dried specimens. The polyelectrolyte complexation process was carried out in sufficient dilute solution to reduce the relative abundance of multichain clusters that can be viewed as pregel clusters in the formation of macroscopic gels. The analysis of the complexes observed in the AFM topographs shows that the chain stiffness of the polyanion is an important factor influencing the relative fraction of morphologies within the three classes of characteristic shapes, globular, linear, and toroidal. In particular, the formation of toroidal structures is found not to be restricted to DNA, but is observed at a sufficiently large persistence length of the compacted semiflexible biopolymers.

Furthermore, we find that compaction of high-molecular-weight xanthan yields a blend of toroids and metastable states. Reduction of the molecular weight of xanthan reduces the fraction of toroids, while annealing of the complexes increases this fraction. In addition to the relation between the chain stiffness and the geometric features of the isolated compacted structures, the observed morphologies of the complexes of the selected polysaccharides follow the trend established by DNA. This indicates that the formation of the complexes at the present level of refinement of the analysis is not affected by specific interactions, but is dominated by the electrostatics and chain stiffness. Results from DNA condensation using a series of spermine and spermine analogues[53] suggest that detailed molecular architecture influences the compaction reaction. The present data of a large uncomplexed fraction of acetan chains indicate that the detailed molecular architecture is important for hindering interactions and that the overall result originates from a detailed balance of interactions that contribute to different extents also in the case of polysaccharides.

**Acknowledgment.** This work is supported by The Norwegian Research Council (Grant Nos. 129104/420, 121894/420, and 134674/140). We are indebted to Dr. Kjell Morten Vårum, Department of Biotechnology, NTNU, Norway, for providing the chitosan samples, and Statoil/Norferm, Stavanger, Norway,

for providing the xanthan sample. The assistance in determination of the molecular weight of some of the samples using SEC-MALLS by Dr. Bjørn E. Christensen, Department of Biotechnology, NTNU, Norway, is gratefully acknowledged.

## References and Notes

(1) Widom, J.; Baldwin, R. L. *J. Mol. Biol.* **1980**, *144*, 431−453.
(2) Arscott, P. G.; Li, A.-Z.; Bloomfield, V. A. *Biopolymers* **1990**, *30*, 619−630.
(3) Plum, G. E.; Arscott, P. G.; Bloomfield, V. A. *Biopolymers* **1990**, *30*, 631−643.
(4) Bloomfield, V. A. *Biopolymers* **1997**, *44*, 269−282.
(5) Golan, R.; Pietrasanta, L. I.; Hsieh, W.; Hansma, H. G. *Biochemistry* **1999**, *38*, 14069−14076.
(6) Fang, Y.; Hoh, J. H. *J. Am. Chem. Soc.* **1998**, *120*, 8903−8909.
(7) Martin, A. L.; Davies, M. C.; Rackstraw, B. J.; Roberts, C. J.; Stolnik, S.; Tendler, S. J. B.; Williams, P. M. *FEBS Lett.* **2000**, *480*, 106−112.
(8) Arscott, P. G.; Ma, C.; Wenner, J. R.; Bloomfield, V. A. *Biopolymers* **1995**, *36*, 345−364.
(9) Fang, Y.; Spisz, T. S.; Hoh, J. H. *Nucleic Acids Res.* **1999**, *27*, 1943−1949.
(10) Raspaud, E.; de la Cruz, M. O.; Sikorav, J.-L.; Livolant, F. *Biophys. J.* **1998**, *74*, 381−393.
(11) Borukhov, I.; Lee, K.-C.; Bruinsma, R. F.; Gelbart, R. F.; Liu, A. J.; Stevens, M. J. *J. Chem. Phys.* **2002**, *117*, 462−480.
(12) Noguchi, H.; Yoshikawa, K. *J. Chem. Phys.* **1998**, *109*, 5070−5077.
(13) Ivanov, V. A.; Stukan, M. R.; Vasilevskaya, V. V.; Paul, W.; Binder, K. *Macromol. Theory Simul.* **2000**, *9*, 488−499.
(14) Kwoh, D. Y.; Coffin, C. C.; Lollo, C. P.; Jovenal, J.; Banaszczyk, M. G.; Mullen, P.; Phillips, A.; Amini, A.; Fabrycki, J.; Bartholomew, R. M.; Brostoff, S. W.; Carlo, D. J. *Biochim. Biophys. Acta* **1999**, *1444*, 171−190.
(15) Noguchi, H.; Yoshikawa, K. *Chem. Phys. Lett.* **1997**, *278*, 184−188.
(16) Stevens, M. J. *Phys. Rev. Lett.* **1999**, *82*, 101−104.
(17) Stevens, M. J. *Biophys. J.* **2001**, *80*, 130−139.
(18) Tang, J. X.; Käs, J. A.; Shah, J. V. *Eur. Biophys. J.* **2001**, *30*, 477−484.
(19) Noguchi, H.; Yoshikawa, K. *J. Chem. Phys.* **2000**, *113*, 854−862.
(20) Schnurr, B.; MacKintosh, F. C.; Williams, D. R. M. *Europhys. Lett.* **2000**, *51*, 279−285.
(21) Sato, T.; Norisuye, T.; Fujita, H. *Polym. J.* **1984**, *16*, 341−350.
(22) Sato, T.; Norisuye, T.; Fujita, H. *Macromolecules* **1984**, *17*, 2696−2700.
(23) Nakasagu, M.; Norisuye, T. *Polym. J.* **1988**, *20*, 939−944.
(24) Borochov, N.; Eisenberg, H. *Biopolymers* **1984**, *23*, 1757−1769.
(25) Hagerman, P. J. *Biopolymers* **1983**, *22*, 811−814.
(26) Smith, S. B.; Cui, Y.; Bustamante, C. *Science* **1996**, *271*, 795−799.
(27) Wenner, J. R.; Williams, M. C.; Rouzina, I.; Bloomfield, V. A. *Biophys. J.* **2002**, *82*, 3160−3169.
(28) Berth, G.; Dautzenberg, H.; Christensen, B. E.; Rother, G.; Smidsrød, O. *Biopolymers* **1996**, *39*, 709−719.
(29) Christensen, B. E.; Smidsrød, O.; Elgsaeter, A.; Stokke, B. T. *Macromolecules* **1993**, *26*, 6111−6120.
(30) Stokke, B. T.; Brant, D. A. *Biopolymers* **1990**, *30*, 1161−1181.
(31) Strand, K. A.; Bøe, A.; Dalberg, P. S.; Sikkeland, T.; Smidsrød, O. *Macromolecules* **1982**, *15*, 570−579.
(32) Smidsrød, O.; Haug, A. *Acta Chem. Scand.* **1968**, *22*, 797−810.
(33) Daune, M. *Molecular Biophysics. Structures in Motion*; Oxford University Press: Oxford, 1999; pp 341−359.
(34) Tyler, J. M.; Branton, D. *J. Ultrastruct. Res.* **1980**, *71*, 95−102.
(35) Stokke, B. T.; Falch, B. H.; Dentini, M. *Biopolymers* **2001**, *58*, 535−547.
(36) Spisz, T. S.; Fang, Y.; Reeves, R. H.; Seymour, C. K.; Bankman, I. N.; Hoh, J. H. *Med. Biol. Eng. Comput.* **1998**, *36*, 667−672.
(37) Zifferer, G.; Olaj, O. F. *J. Chem. Phys.* **1994**, *100*, 636−639.
(38) Zifferer, G. *J. Chem. Phys.* **1998**, *109*, 3691−3698.
(39) Fang, Y.; Hoh, J. H. *FEBS Lett.* **1999**, *459*, 173−176.
(40) Stokke, B. T.; Elgsaeter, A.; Skjåk-Bræk, G.; Smidsrød, O. *Carbohydr. Res.* **1987**, *160*, 13−18.
(41) Stokke, B. T.; Smidsrød, O.; Elgsaeter, A. *Biopolymers* **1989**, *28*, 617−637.
(42) Danielsen, S.; Vårum, K. M.; Stokke, B. T. Manuscript in preparation.
(43) Lin, Z.; Wang, C.; Feng, X.; Liu, M.; Li, J.; Bai, C. *Nucleic Acids Res.* **1998**, *26*, 3228−3234.
(44) Grosberg, A. Y.; Nguyen, T. T.; Shklovski, B. I. *Rev. Mod. Phys.* **2002**, *74*, 329−345.
(45) Dautzenberg, H. *Macromolecules* **1997**, *30*, 7810−7815.
(46) Jansson, P. E.; Lindberg, J.; Wimalasiri, S.; Dankert, M. A. *Carbohydr. Res.* **1993**, *245*, 303−310.
(47) Christensen, B. E.; Smidsrød, O.; Stokke, B. T. *Carbohydr. Polym.* **1994**, *25*, 25−29.
(48) Tricot, M. *Macromolecules* **1984**, *17*, 1698−1704.
(49) Schnurr, B.; Gittes, F.; MacKintosh, F. C. *Phys. Rev. E* **2002**, *65*, 161904-161-13.
(50) Park, S. Y.; Harries, D.; Gelbart, W. M. *Biophys. J.* **1998**, *75*, 714−720.
(51) Shimada, J.; Yamakawa, H. *Macromolecules* **1984**, *17*, 689−698.
(52) Shen, M. R.; Downing, K. H.; Balhorn, R.; Hud, N. V. *J. Am. Chem. Soc.* **2000**, *122*, 4833−4834.
(53) Vijayanathan, V.; Thomas, T.; Shirahata, A.; Thomas, T. J. *Biochemistry* **2001**, *40*, 13644−13651.
(54) Atkins, E. D. T.; Nieduszynski, I. A.; Mackie, W.; Parker, K. D.; Smolko, E. E. *Biopolymers* **1973**, *12*, 1865−1878.
(55) Atkins, E. D. T.; Nieduszynski, I. A.; Mackie, W.; Parker, K. D.; Smolko, E. E. *Biopolymers* **1973**, *12*, 1879−1887.
(56) Haug, A. Composition and properties of alginates. Thesis, Norwegian Institute of Technology, Trondheim, Norway, 1964.
(57) Morris, V. J.; Brownsey, G. J.; Cairns, P.; Chilvers, G. R.; Miles, M. J. *Int. J. Biol. Macromol.* **1989**, *11*, 326−328.
(58) Record, M. T.; Anderson, C. F.; Lohman, T. M. *Q. Rev. Biophys.* **1978**, *11*, 103−178.
(59) Bloomfield, V. A.; Crothers, D. M.; Tinoco, I. *Nucleic Acids. Structures, properties and functions*; University Science Books: Sausalito, CA, 2000; pp 13−43.
(60) Okuyama, K.; Arnott, S.; Moorhouse, R.; Walkinshaw, M. D.; Atkins, E. D. T.; Wolf-Ullish, C. *Am. Chem. Soc. Symp. Ser.* **1980**, *141*, 411−427.
(61) Zhang, L.; Takematsu, T.; Norisuye, T. *Macromolecules* **1987**, *20*, 2882−2887.
(62) Young, S.-L.; Martino, M.; Kienzle-Sterzer, C.; Torres, J. A. *J. Sci. Food Agric.* **1994**, *64*, 121−127.
(63) Moe, S. T.; Elgsaeter, A.; Skjåk-Bræk, G.; Smidsrød, O. *Carbohydr. Polym.* **1993**, *20*, 263−268.
(64) Cölfen, H.; Berth, G.; Dautzenberg, H. *Carbohydr. Polym.* **2001**, *45*, 373−383.
(65) Okuyama, K.; Noguchi, K.; Miyazawa, T.; Yui, T.; Ogawa, K. *Macromolecules* **1997**, *30*, 5849−5855.
(66) Brant, D. A.; Flory, P. J. *J. Am. Chem. Soc.* **1965**, *87*, 2788−2800.
(67) Grasdalen, H.; Larsen, B.; Smidsrød, O. *Carbohydr. Res.* **1981**, *89*, 179−191.
(68) Vårum, K. M.; Anthonsen, M. W.; Grasdalen, H.; Smidsrød, O. *Carbohydr. Res.* **1991**, *211*, 17−23.
(69) Vårum, K. M.; Anthonsen, M. W.; Grasdalen, H.; Smidsrød, O. *Carbohydr. Res.* **1991**, *217*, 19−27.